submitted to *Geophys. J. Int.*

Polarization Effects of Seismic Waves on the Basis of Radiative Transport Theory

Guillaume Bal* and Miguel Moscoso†

*Department of Mathematics, University of Chicago, Chicago, IL 60637,USA

†Department of Mathematics, Stanford University, Stanford CA 94305,USA

SUMMARY
Radiative transfer theory provides a good framework for the study of multiple scattering in the randomly inhomogeneous lithosphere. Envelopes of high-frequency seismograms (mainly S-coda waves) of local earthquakes have been synthesized on the basis of this theory, and inversions for some Earth's parameters such as intrinsic attenuation, scattering attenuation, and degree of non-isotropic scattering, have been carried out. However, they have often assumed a scalar model because of its mathematical relative simplicity. The simplification amounts to neglecting the polarized nature of the underlying motion. This approach is only valid for long lapse times when the energy becomes unpolarized due to high order scattering, and cannot be justified by only assuming that the source is unpolarized. We show that single scattering of unpolarized sources can be up to 80% polarized. Using a Monte Carlo method for transverse waves, we study the time evolution of the polarization due to multiple scattering. This additional piece of information should be valuable for understanding the physics of wave motion and the properties of the Earth's lithosphere.

Key words: coda, polarization, scattering, heterogeneity, radiative transfer theory, Monte Carlo method

1 INTRODUCTION

Coda waves analysis has attracted a lot of interest in recent years. The coda is composed of scattered waves that sample the random medium in a similar way to the averaging of direct waves over a seismic network. Therefore, their study provides a good tool to understand the random inhomogeneities of the Earth's lithosphere and estimate its properties.

Since the pioneering work of Aki, 1969, on the seismic coda of local earthquakes, many authors [e.g., Aki & Chouet, 1975; Sato, 1977; Frankel & Wennerberg, 1987; Herraiz & Espinosa, 1987] have used phenomenological models to fit the total scattering coefficient and the coda-wave attenuation to real S-coda data. More recently, theoretical [e.g., Wu, 1985; Wu & Aki, 1988; Shang & Gao, 1988; Zeng et al., 1991; Sato , 1993; Sato, 1994]; and numerical studies [e.g., Gusev & Abubakirov, 1987; Hosiba, 1991; Margerin et al., 1998] based on the radiative transfer theory [Chandrasekhar, 1960; Ishimaru, 1978] have been applied to synthesize coda envelopes. In all those studies, the vector nature of the underlying wave motion is not taken into account, and a simplified scalar version of the motion is analyzed. The simplification amounts to neglecting the polarized nature of shear waves. In addition, isotropic scattering is almost always assumed.

The aim of the present paper is to analyze the polarization effects of shear waves. Specifically, we follow the model derived in Ryzhik et al., 1996, for the propagation of elastic wave energy in random media to compute the spatio-temporal distributions of the energy density and of the rate of polarization. Starting from the full linear elastic wave equations, they derive a system of coupled radiative transfer equations for the angularly resolved P-wave energy density and S-wave coherence matrix. Based on the observation that S-coda waves are composed primarily of S-waves [Tsujiura, 1978] we do not take into account the coupling between P- and S-waves. These observations are supported by the theory developed by Aki, 1992, Zeng, 1993, and Papanicolaou et al., 1996, where the ratio of the energy conversion coefficients as functions of the P- to S-wave velocity ratio γ is given. In practice, $\gamma \approx \sqrt{3}$. The scattered energy conversion from P- to S-waves is $2\gamma^4 \approx 18$ times larger than the S- to P-wave conversion. It is also shown in Sato, 1984, that the ratio of the radiated S-wave energy to the P-wave energy from a point shear dislocation is $1.5\gamma^5 \approx 23.4$. Both factors lead to a preponderance of S-waves.

The spatio-temporal distributions of the energy and the polarization rate are computed by a Monte Carlo method. Unlike scalar equations, matrix-valued equations do not have a direct probabilistic representation suitable for Monte Carlo simulation. We follow the recent probabilistic representation of polarized radiative transfer equations given in Bal et al., 1999, to present a simple implementation for elastic radiative transfer; see also Bal & Moscoso, 1999 for an application to electro-magnetic radiative transfer.

In this paper, we consider media with random fluctuations in the density and in the Lamé parameters, and show that the corresponding underlying scattering laws provide different energy coda envelopes. We also present the spatio-temporal distribution of the polarization and depolarization phenomena of S-waves. We will show that the these effects are very important for local earthquakes, and that they disappear only for large lapse times. In addition, we will see that they are very sensitive to the scattering law.

Our paper is organized as follows. We describe in section 2 our model for S-wave propagation. We show in section 3 how to solve it by Monte Carlo method. We study the single scattering approximation assuming initially unpolarized waves in section 4. In section 5 we compute the effects of multiple scattering in the free space using the Monte Carlo method. In section 6, we address the half space and slab problems, and show the rate of polarization at the free surface. The last section contains our conclusions. We also include three Appendices, where we address the details of the probability scattering density, the single scattering approximation, and the implementation of the Monte Carlo method.

2 RADIATIVE TRANSFER EQUATIONS FOR ELASTIC WAVES

Shear waves cannot be described by a scalar density. They require a 2×2 non-negative hermitian matrix

$$W(t, \mathbf{x}, \mathbf{k}) = \frac{1}{2} \begin{pmatrix} I+Q & U+iV \\ U-iV & I-Q \end{pmatrix}, \tag{1}$$

which accounts for their polarized structure. The parameter I describes the total energy of the shear waves, whereas Q, U, and V describe its polarization. Fully polarized waves satisfy the relation $I^2 = Q^2 + U^2 + V^2$, or equivalently $\det W = 0$. The polarization of a fully polarized transverse wave is characterized by the end point of an arrow representing the wave motion. In the general case, the arrow describes an ellipse with unequal principal axes $\mathbf{e}_1$ and $\mathbf{e}_2$ and making an angle χ with a chosen orthogonal system of reference $(\mathbf{e}_l, \mathbf{e}_r)$ transverse to the wave motion [see Fig. 1(a)]. The Stokes parameter Q is defined as the

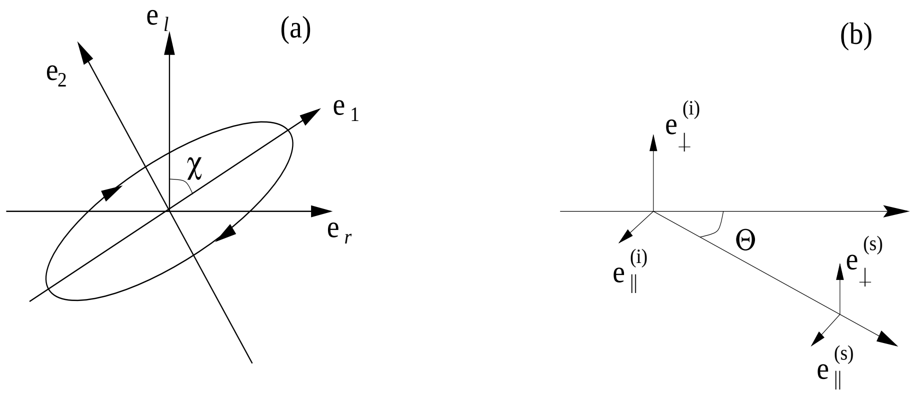

Figure 1. (a) Polarization ellipse for a transverse wave. (b) Coordinate system for the polarization parameters of the incident and scattered waves in single scattering. The scattering plane is defined by the incident and scattered directions, and $\|$ and $\perp$ stand for parallel and perpendicular directions, respectively, in the planes transverse to the incident and scattered waves.

difference between the energy of the waves linearly polarized along the $\mathbf{e}_l$ direction and along the $\mathbf{e}_r$ direction. The same holds for U but with reference to two directions rotated by 45° respect to $(\mathbf{e}_l, \mathbf{e}_r)$. At last, V determines the difference between the energy densities that are right- or left-hand circularly polarized. Then, we can write

$$\begin{aligned} I &= I_l + I_r, \qquad Q = I_l - I_r, \\ U &= [I_l - I_r] \tan 2\chi, \qquad V = [I_l - I_r] \tan 2\beta \sec 2\chi, \end{aligned} \tag{2}$$

where β is the angle [between 0 and $\pi/2$] whose tangent is the ratio of the principal axes of the ellipse. Consequently, for linearly polarized waves V is equal to 0. When the end point of the vector moves completely randomly, the wave is unpolarized. However, as we will see, the waves are generally in intermediate states of polarization, i.e., partially polarized. In this case, we have that $I^2 \geq Q^2 + U^2 + V^2$.

Here, we consider a homogeneous constant-velocity background medium with random inhomogeneities on the scale of the wavelength. Inhomogeneities are variations of the elastic coefficients and mass density due to changes in material composition or to the presence of cracks. Due to these fluctuations, a wave with wave vector $\mathbf{k}'$ at a point $\mathbf{x}$ may be scattered into any direction $\hat{\mathbf{k}}$ with wave vector $\mathbf{k}$. We do not consider P to S conversion and dissipation. With these assumptions, the energy conservation is expressed by the transport equation [Ryzhik et al., 1996]

$$\frac{1}{v}\frac{\partial W(t,\mathbf{x},\mathbf{k})}{\partial t} + \hat{\mathbf{k}} \cdot \nabla_{\mathbf{x}} W(t,\mathbf{x},\mathbf{k}) = \int \sigma(\mathbf{k},\mathbf{k}')[W(\mathbf{k}')]d\mathbf{k}' - \Sigma(\mathbf{k}) W(t,\mathbf{x},\mathbf{k}), \tag{3}$$

where $\mathbf{k} = |\mathbf{k}|\hat{\mathbf{k}}$, v is the velocity of the homogeneous background, and $\nabla_{\mathbf{x}} = (\frac{\partial}{\partial x}, \frac{\partial}{\partial y}, \frac{\partial}{\partial z})^t$.

The local speed of propagation of shear waves is given by $v(\mathbf{x}) = \sqrt{\mu(\mathbf{x})/\rho(\mathbf{x})}$. However, complete information about the spatial dependence of the elastic constant μ and the density ρ is not available for the whole Earth's lithosphere, and a statistical treatment is necessary. Assuming a statistically homogeneous and statistically isotropic medium, Ryzhik et al., 1996, wrote the differential scattering cross-section in terms of the power spectral densities $\hat{R}_{\mu\mu}$ and $\hat{R}_{\rho\rho}$ and $\hat{R}_{\mu\rho}$ of the inhomogeneities. In this paper, we assume that $\hat{R}_{\mu\rho} = 0$. Then, the differential scattering tensor has the form

$$\sigma(\mathbf{k},\mathbf{k}')[W(\mathbf{k}')] = [\sigma_{\rho\rho} T(\mathbf{k},\mathbf{k}') W(\mathbf{k}') T(\mathbf{k}',\mathbf{k}) + \sigma_{\mu\mu} \Gamma(\mathbf{k},\mathbf{k}') W(\mathbf{k}') \Gamma(\mathbf{k}',\mathbf{k})], \tag{4}$$

where the scalar functions

$$\sigma_{\rho\rho} = \frac{\pi}{2} v|\mathbf{k}|^2 \hat{R}_{\rho\rho}(|\mathbf{k}-\mathbf{k}'|)\delta(v|\mathbf{k}| - v|\mathbf{k}'|), \quad \sigma_{\mu\mu} = \frac{\pi}{2} v|\mathbf{k}|^2 \hat{R}_{\mu\mu}(|\mathbf{k}-\mathbf{k}'|)\delta(v|\mathbf{k}| - v|\mathbf{k}'|), \tag{5}$$

are the differential scattering cross-sections due to fluctuations in the density ρ and the Lamé parameter μ, respectively. Notice that the delta function in Eq. (5) implies that the frequencies are unchanged by scattering. Therefore, different frequencies satisfy uncoupled equations. We consequently assume that the modulus $|\mathbf{k}|$ of the wave number of our initial condition $W_0(\mathbf{x}, \mathbf{k})$ is fixed. Note that it determines the differential cross-sections and the total scattering cross-section defined below.

The 2×2 matrices $T(\mathbf{k}, \mathbf{k}')$ and $\Gamma(\mathbf{k}, \mathbf{k}')$ are defined by

$$\begin{aligned} T_{ij}(\mathbf{k}, \mathbf{k}') &= (\mathbf{z}^{(i)}(\mathbf{k}) \cdot \mathbf{z}^{(j)}(\mathbf{k}')) \\ \Gamma_{ij}(\mathbf{k}, \mathbf{k}') &= (\hat{\mathbf{k}} \cdot \hat{\mathbf{k}}')(\mathbf{z}^{(i)}(\mathbf{k}) \cdot \mathbf{z}^{(j)}(\mathbf{k}')) + (\hat{\mathbf{k}} \cdot \mathbf{z}^{(j)}(\mathbf{k}'))(\hat{\mathbf{k}}' \cdot \mathbf{z}^{(i)}(\mathbf{k})), \end{aligned} \tag{6}$$

with the vectors $(\hat{\mathbf{k}}, \mathbf{z}^{(1)}(\mathbf{k}), \mathbf{z}^{(2)}(\mathbf{k}))$,

$$\hat{\mathbf{k}} = \begin{pmatrix} \sin\theta\cos\phi \\ \sin\theta\sin\phi \\ \cos\theta \end{pmatrix}, \ \mathbf{z}^{(1)}(\mathbf{k}) = \begin{pmatrix} \cos\theta\cos\phi \\ \cos\theta\sin\phi \\ -\sin\theta \end{pmatrix}, \ \mathbf{z}^{(2)}(\mathbf{k}) = \begin{pmatrix} -\sin\phi \\ \cos\phi \\ 0 \end{pmatrix}, \tag{7}$$

forming a local orthonormal basis in $\mathbb{R}^3$. The differential scattering tensor (4) and the total scattering cross section are related by

$$\int_{\mathbb{R}^3} \sigma(\mathbf{k}', \mathbf{k})[\mathbb{I}_2] d\mathbf{k}' = \Sigma(\mathbf{k})\mathbb{I}_2 \ , \tag{8}$$

where $\mathbb{I}_2$ is the 2×2 identity matrix, and

$$\begin{aligned} \Sigma(\mathbf{k}) = \frac{\pi^2|\mathbf{k}|^4}{2} \int_{-1}^{1} d(\cos\Theta) \, \{\hat{R}_{\mu\mu}(|\mathbf{k}|\sqrt{2-2\cos\Theta})[(\cos^2\Theta + \sin^2\Theta)^2 + \cos^2\Theta] \\ + \hat{R}_{\rho\rho}(|\mathbf{k}|\sqrt{2-2\cos\Theta})[1+\cos^2\Theta]\} \ . \end{aligned} \tag{9}$$

Here, $\cos\Theta = \hat{\mathbf{k}} \cdot \hat{\mathbf{k}}'$. Although, expressions (8)and (9) can be check by direct computation, we can motivate the functional dependence. The assumption of statistically isotropic medium implies that the scattering coefficient depends only on $\hat{\mathbf{k}} \cdot \hat{\mathbf{k}}'$, leaving a trivial integration in azimuthal angle. Moreover, assuming that $\hat{R}_{\mu\mu} = 0$ [respectively $\hat{R}_{\rho\rho} = 0$], an incident unpolarized beam scattering in a direction making and angle Θ with the direction of incidence becomes partially plane-polarized with a ratio of the energy densities equal to $1/\cos^2\Theta$ [respectively $(\cos^2\Theta - \sin^2\Theta)^2/\cos^2\Theta$] in directions perpendicular and parallel to the plane of scattering, which is spanned by the incident and scattered directions. This feature will be important when we analyze the single scattering approximation.

Equation (3) is a good approximation of the wave energy transport when the typical wavelength is short compared to the macroscopic properties of the medium and the correlation length of the inhomogeneities is of the same order as the wavelength. In addition, fluctuations of the heterogeneities must not be so strong as to cause localization. It is important to observe that the coherence matrix W as well as the radiative transfer equation (3) are represented in a given orthonormal basis $(\mathbf{e}_x, \mathbf{e}_y, \mathbf{e}_z)$. The change of representation by rotation of the basis is not straightforward[Chandrasekhar, 1960].

For the calculations that follow, it is convenient to render Eq. (3) dimensionless by normalizing time, length, and related quantities in terms of the S-wave velocity v and the mean free path $1/\Sigma$ (about $4km/s$ and of the order of $100km$, respectively, for frequencies of $1-30$ Hz [Sato and Fehler, 1997]). The initial condition we consider in this paper is an unpolarized isotropic source term with frequency ω of the form $W_0(\mathbf{x}, \mathbf{k}) = w_0\mathbb{I}_2\delta(\mathbf{x})$. Then, we define the following adimensionalized quantities

$$\tilde{t} = v\Sigma t, \qquad \tilde{\mathbf{x}} = \Sigma \mathbf{x}, \qquad \tilde{\mathbf{k}} = \frac{v}{\omega}\mathbf{k} \qquad \tilde{W}(\tilde{t}, \tilde{\mathbf{x}}, \tilde{\mathbf{k}}) = \frac{W(t, \mathbf{x}, \mathbf{k})}{w_0} \ . \tag{10}$$

After integration over the modulus of the wave vector in Eq. (3) using Eq. (5), and dropping the symbol ˜ for simplicity, we obtain the dimensionless equation

$$\begin{aligned} &\frac{\partial W(t,\mathbf{x},\mathbf{k})}{\partial t} + \mathbf{k}\cdot\nabla_{\mathbf{x}} W(t,\mathbf{x},\mathbf{k}) + W(t,\mathbf{x},\mathbf{k}) = \frac{15}{8\pi(5\hat{R}_{\rho\rho} + 3\hat{R}_{\mu\mu})} \times \\ &\int_{|\mathbf{k}'|=1} \Big(\hat{R}_{\rho\rho} T(\mathbf{k},\mathbf{k}') \tilde{W}(t,\mathbf{x},\mathbf{k}') T(\mathbf{k}',\mathbf{k}) + \hat{R}_{\mu\mu} \Gamma(\mathbf{k},\mathbf{k}') \tilde{W}(t,\mathbf{x},\mathbf{k}') \Gamma(\mathbf{k}',\mathbf{k}) \Big) d\mathbf{k}' \end{aligned} \tag{11}$$

Here we have assumed that $\hat{R}_{\rho\rho} \equiv Cte$ and $\hat{R}_{\mu\mu} \equiv Cte$. Moreover, we see that real and imaginary parts of W are uncoupled since the matrix T is real. This means that the circularly polarized component of the waves evolves independently of the other components. Therefore, we assume without loss of generality that $V = 0$, which corresponds to the case of linearly polarized shear waves. In the sequel we consider only the dimensionless radiative transfer equation (11).

To summarize, shear waves cannot be described by a scalar quantity accurately, and requires the 2×2 matrix (1), which accounts for their polarized structure. We want to analyze this feature in the paper and deal with the polarization and depolarization effects of S-waves. To simplify the analysis, we will consider two examples, (i) fluctuating Lamé parameter μ and constant density ρ, and (ii) constant μ and fluctuating ρ. We will refer to them as the first and second case, respectively.

3 MONTE CARLO METHOD

We want to solve (11) by the Monte Carlo method. This method enables us to deal with complicated 3D geometries with reasonable storage requirements. It is in addition relatively easy to implement. For those reasons, it is very popular in radiation transport, heat transfer, and nuclear reactor theory [Kalos & Whitlock, 1986; Spanier & Gelbard, 1969]. The radiative transfer equations for scalar waves have the same structure as transport equations for particles. The central characteristic of Monte Carlo methods is to simulate the behavior of one particle at a time. The average over a large number of realizations of particle paths yields an estimate of the particle probability density.

The simulation of the particle trajectories is threefold: (i) description of the particle trajectories between successive scattering events, (ii) estimation of the time of the next scattering with the underlying medium, and (iii) at the time when the particle undergoes scattering, computation of the outgoing velocity of the particle. The last two steps are random processes.

As it is, this method does not hold for coherence matrices, whose entries do not correspond only to energies, but also to polarization parameters. Moreover, the probability distribution of the outgoing velocity after scattering does not only depend on the incident direction, as for scalar particle transport, but also on its state of polarization.

Nonetheless, it is possible to adapt these ideas for S-waves by considering the polarization parameters as independent variables, i.e., each particle will be characterized by its position $X(t)$, velocity $K(t)$, and polarization state $\mathcal{P}(t)$. We refer to Bal et al., 1999, for more details. Let us summarize here the main ideas.

We rewrite the matrix W as

$$W(t,\mathbf{x},\mathbf{k}) = \frac{I}{2}\begin{pmatrix} 1+Q/I & U/I \\ U/I & 1-Q/I \end{pmatrix} = \frac{I}{2}\left[\mathbb{I}_2 + \mathcal{P}\right] \ , \tag{12}$$

where

$$\mathcal{P} = \begin{pmatrix} p_1 & p_2 \\ p_2 & -p_1 \end{pmatrix} = \begin{pmatrix} Q/I & U/I \\ U/I & -Q/I \end{pmatrix} \ . \tag{13}$$

Note that the intensity I is the trace of $W(t, \mathbf{x}, \mathbf{k})$. In addition to the position $X(t)$ and wave vector (velocity) $K(t)$ we now have a pair of polarization processes $p_1(t)$ and $p_2(t)$ which describe the polarization parameters Q and U [see equation (13)]. The position $X(t)$ is continuous in space, while the velocity $K(t)$ and polarization parameters $\mathcal{P}(t)$ jump at the scattering times.

The evolution $(X(t), K(t), \mathcal{P}(t))$ of each particle follows the following rules. It evolves along straight characteristics between successive scatterings:

$$\frac{dX}{dt} = K(t), \qquad \frac{dK}{dt} = 0, \qquad \frac{dp_i}{dt} = 0, \quad i = 1, 2. \tag{14}$$

At time s, the probability that the next scattering takes place after time t follows the Poisson distribution

$$P(\text{Time of Next Scattering} > t) = e^{-(t-s)}. \tag{15}$$

When a scattering event takes place, we have to define the outgoing velocity and polarization parameters. The probability density for a jump from wave vector $\mathbf{k}$ and polarization matrix $\mathcal{P}$ into wave vector $\mathbf{k}'$ and polarization matrix $\mathcal{P}'$ is

$$\pi(\mathbf{k}, \mathcal{P}, \mathbf{k}', \mathcal{P}') = C \mathrm{Tr} \left\{ S(\mathbf{k}', \mathbf{k})[\mathbb{I}_2 + \mathcal{P}] S(\mathbf{k}, \mathbf{k}') \right\} \ , \tag{16}$$

where the matrix S stands for T or Γ, C is a normalization constant, and Tr stands for trace of the matrix. The matrix of the scattered polarization parameters $\mathcal{P}_s(\mathbf{k}, \mathcal{P}, \mathbf{k}')$, which is symmetric and has null trace, is determined by [Bal et al., 1999]

$$\frac{1}{2}(\mathbb{I}_2 + \mathcal{P}_s) = \frac{S(\mathbf{k}', \mathbf{k})[\mathbb{I}_2 + \mathcal{P}] S(\mathbf{k}, \mathbf{k}')}{\mathrm{Tr}\{S(\mathbf{k}', \mathbf{k})[\mathbb{I}_2 + \mathcal{P}] S(\mathbf{k}, \mathbf{k}')\}}. \tag{17}$$

For the reader's convenience we have postponed to Appendix A the computation of the probability measure π and the scattered polarization parameters. We see in these expressions that the jump probability does not depend on the outgoing polarization parameters $\mathcal{P}'$ and that the outgoing polarization parameters are functions of the incoming and outgoing velocities $\mathbf{k}'$ and $\mathbf{k}$, and of the incoming polarization parameters $\mathcal{P}$.

The history of each particle is constructed as follows. The history $(X(t), K(t), \mathcal{P}(t))$ starts at $(\mathbf{x}_0, \mathbf{k}_0, \mathcal{P}^0)$. The time of first scattering τ_1 is given by the probability density (15). The process follows (14) between $0 \leq t < \tau_1$. At τ_1 the process jumps to a new velocity $K(\tau_1)$ and a new polarization state $\mathcal{P}(\tau_1)$ according to (16) and (17), respectively. Then, a new scattering time τ_2 is obtained according to (15). The process is continued in an obvious manner until a final time T_f.

The implementation of the Monte Carlo method is given in appendix C. The validity of our code was checked by comparing the numerical results with the analytic single scattering solution computed in section 4 and with the diffusion solution for large lapse times. The agreement was perfect in both cases.

4 SINGLE SCATTERING

The application of single scattering models [e.g., Aki, 1969; Sato, 1977] is based on the assumption of weak scattering, for which the mean free path [equal to 1 in our adimensional units] is much longer than the source-receiver distance. In addition to being a fairly good approximation, it also provides us with a good understanding of how polarization is generated by the interaction of unpolarized waves with the random heterogeneities. Therefore, this phenomenon may prove extremely useful in the estimation of the characteristics of the Earth's lithosphere from high frequency seismic data.

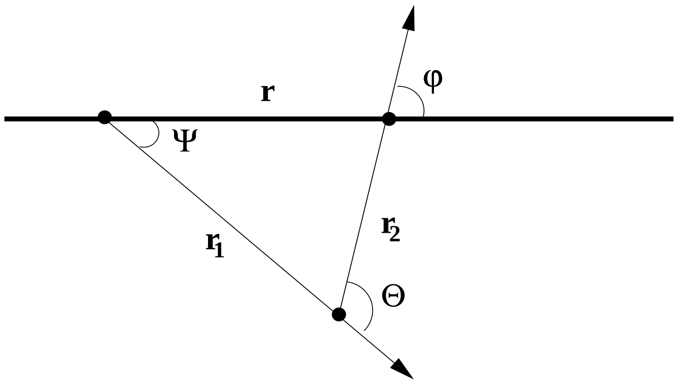

Figure 2. Single scattering geometry.

Here, we consider heterogeneities of the Earth's lithosphere due to fluctuations of the Lamé parameter μ and to fluctuations of the density ρ, successively. We do not consider correlations between both fluctuations. Let us refer to them as the first and second case. We will distinguish between them by using the superscripts μ and ρ, respectively.

We calculate the spatio-temporal distribution of the intensity and of the degree of polarization for the two cases using the relative simplicity of the spherical geometry [see Fig. 2]. Our point source spherically radiates unpolarized energy, which is received at time t, after single scattering, at a point located at a distance r from the source.

In the subsequent section, it is more convenient to use the energy densities $I_{\|}$ and $I_{\perp}$ in directions parallel and perpendicular respectively to the plane of scattering (which contains the incident and scattered directions; see Fig. 1(b)) than the parameters I and Q in (1). Then, we denote the incident energy by the vector

$$J = (I_{\|}, I_{\perp}, U)$$

since we have assumed that $V = 0$. The scattered energy density in the direction Θ is proportional to $M^{\mu,\rho}J$ where M^{μ} and M^{ρ} denote the phase matrix for the fluctuations in the Lamé parameter and for the fluctuations in the density, respectively. They are given by

$$\begin{aligned} M^{\mu} &= \begin{pmatrix} [\cos^2\Theta - \sin^2\Theta]^2 & 0 & 0 \\ 0 & \cos^2\Theta & 0 \\ 0 & 0 & \cos\Theta[\cos^2\Theta - \sin^2\Theta] \end{pmatrix} \\ M^{\rho} &= \begin{pmatrix} \cos^2\Theta & 0 & 0 \\ 0 & 1 & 0 \\ 0 & 0 & \cos\Theta \end{pmatrix} . \end{aligned} \tag{18}$$

For unpolarized source, $I_{\|} = I_{\perp} = \frac{1}{2}I$ and $U = 0$. Notice that after single scattering U remains equal to 0, and the energy densities of the scattered waves in directions parallel and perpendicular respectively to the plane of scattering are in the ratio $[\cos^2\Theta - \sin^2\Theta]^2$ to $\cos^2\Theta$ for the first case, and $\cos^2\Theta$ to 1 for the second.

To compute the energy density and the degree of polarization arriving with angle φ at a distance r from the source at time t, we need to know the relation between the scattering angle Θ, the distance $r_1 \equiv |\mathbf{r}_1|$ where the scattering took place, and the direction φ; see Fig. 2. After some algebra we find that

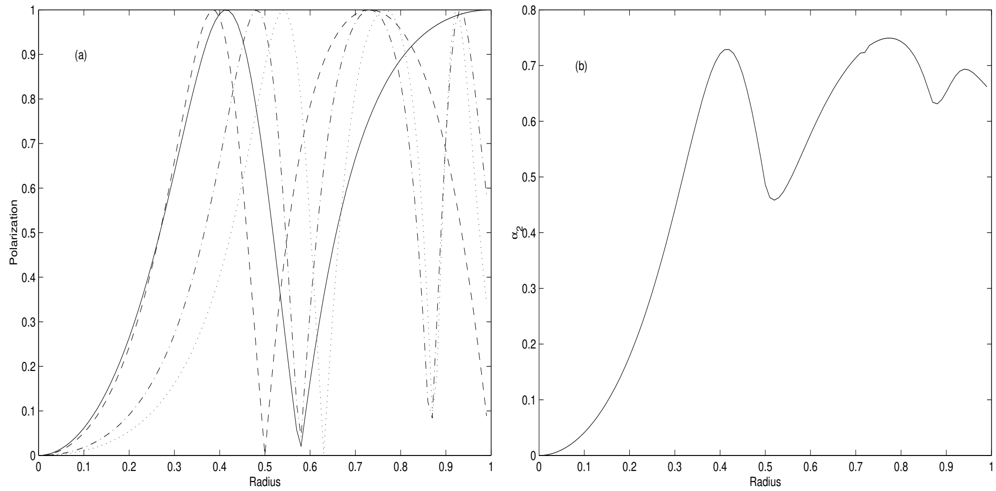

Figure 3. (a) Spatial distribution of the rate of polarization $\alpha_1^{\mu}(r,\varphi,1)$ for $\varphi=\pi/2$ (solid line), $\varphi=\pi/3$ (dashed line), $\varphi=\pi/6$ (dash-dotted line) and $\varphi=\pi/8$ (dotted line). (b) Spatial distribution of the averaged polarization $\alpha_2^{\mu}(r,1)$.

$$\cos[\Theta(r,\varphi,t)] = \frac{2r^2\sin^2\varphi}{r^2-2rt\cos\varphi+t^2} - 1, \qquad r_1(r,\varphi,t) = \frac{r^2-2rt\cos\varphi+t^2}{2(t-r\cos\varphi)} \,. \tag{19}$$

As discussed in the previous paragraph, the polarization α and the energy density I are given by

$$\alpha^{\mu}(r,\varphi,t) = \frac{(\cos^2\Theta-\sin^2\Theta)^2-\cos^2\Theta}{(\cos^2\Theta-\sin^2\Theta)^2+\cos^2\Theta}\,, \qquad \alpha^{\rho}(r,\varphi,t) = \frac{1-\cos^2\Theta}{1+\cos^2\Theta}\,, \tag{20}$$

$$I^{\mu}(r,\varphi,t) = \frac{1}{8\pi r_1(t-r\cos\varphi)}\frac{5}{4}[(cos^2\Theta-sin^2\Theta)^2+cos^2\Theta]\,, \tag{21}$$

$$I^{\rho}(r,\varphi,t) = \frac{1}{8\pi r_1(t-r\cos\varphi)}\frac{3}{4}[1+cos^2\Theta]\,. \tag{22}$$

Here r_1 and Θ are given by (19). The common factor in $I^{\mu,\rho}$ comes from the geometrical spread of the energy density from the source to the point r. Its derivation is explained in Appendix B.

In Fig. 3(a) and Fig. 4(a), we show the spatial distribution of the polarization after one scattering for different angles φ for the first and second case, respectively. We clearly see that the polarization pattern enables us to distinguish between both cases. In the first case, we observe two or three maxima, depending on the angle φ, where the degree of polarization equals 1 (fully polarized energy), with minima in between where the degree of polarization is close to zero (unpolarized energy). In the second case, the polarization is smoother with only one maximum in the interval $[0,1]$. The average rate of polarization

$$\alpha_2^{\mu,\rho}(r,t) = \frac{1}{2}\int_0^{\pi} |\alpha^{\mu,\rho}(r,\varphi,t)|\sin(\varphi)d\varphi\,, \tag{23}$$

is plotted in Fig. 3(b) and Fig. 4(b). Observe that $\alpha_2^{\mu,\rho}$ exactly vanishes at the source location. This is because the scattering angle is π for all directions φ and because unpolarized beams scattered in the back direction remain unpolarized. Also note the three peaks in Fig. 3(b), while only one is present in Fig. 4(b).

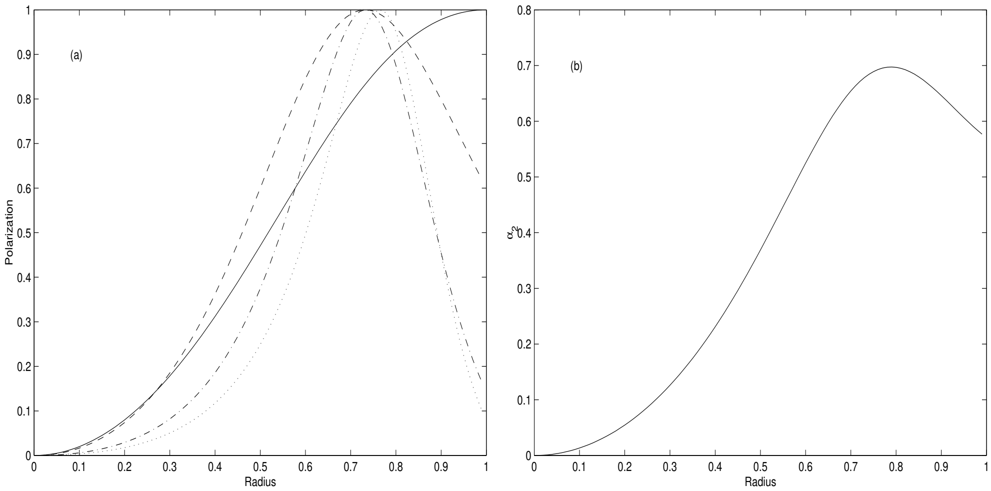

Figure 4. (a) Spatial distribution of the rate of polarization $\alpha_1^\rho(r,\varphi,1)$ for $\varphi=\pi/2$ (solid line), $\varphi=\pi/3$ (dashed line), $\varphi=\pi/6$ (dash-dotted line) and $\varphi=\pi/8$ (dotted line). (b) Spatial distribution of the average polarization $\alpha_2^\rho(r,1)$.

Although (23) seems to be a natural averaged quantity over directions, we prefer

$$\alpha_1^{\mu,\rho}(r,t)=\frac{\displaystyle\int_0^\pi |\alpha^{\mu,\rho}(r,\varphi,t)| I^{\mu,\rho}(r,\varphi,t)\sin(\varphi)d\varphi}{\displaystyle\int_0^\pi I^{\mu,\rho}(r,\varphi,t)\sin(\varphi)d\varphi}\ , \tag{24}$$

which represents the percentage of fully polarized diffuse energy. It also behaves better than α_2 numerically for multiple scattering computations (see section 5), because the directions with more particles, for which the resolution is better, are more represented. This is particularly important for long time computations, where most of the particles remain close to the location of the source.

We have plotted in Fig. 5 the spatio-temporal distribution of α_1^μ (solid line) and α_1^ρ (dashed line). In both cases the maximal value of the degree of polarization is around 0.8. This means that up to 80% of the energy is polarized after single scattering. We see that the difference between both cases is again clear. In the first case (solid line), a first peak is reached very quickly (see Fig. 5(b)), while fluctuations in the density ρ (dashed line) do not generate polarized waves at this time. The second peak coincides in both cases. We also observe that the degree of polarization α_1^ρ decreases monotonously to zero, while α_1^μ has a third peak. At that time, the percentage of fully polarized energy differs between the two cases by a factor greater than 2. In Appendix B, we have derived analytical expressions for $\alpha_1^\rho(r,t)$ and $I^\rho(r,t)$.

We have represented in Fig. 6 the spatio-temporal distribution of the energy density for scattering due to fluctuating μ (solid line), for scattering due to fluctuating ρ (dashed line), and for isotropic scattering (dotted line). We see that in the three cases the scattering generates a logarithmic blow up of the intensity near $r=t$, as is typical for single scattering [Sato & Fehler, 1997]. However, more intensity is concentrated in the vicinity of the source for the scattering generated by the fluctuations of μ than for the other cases.

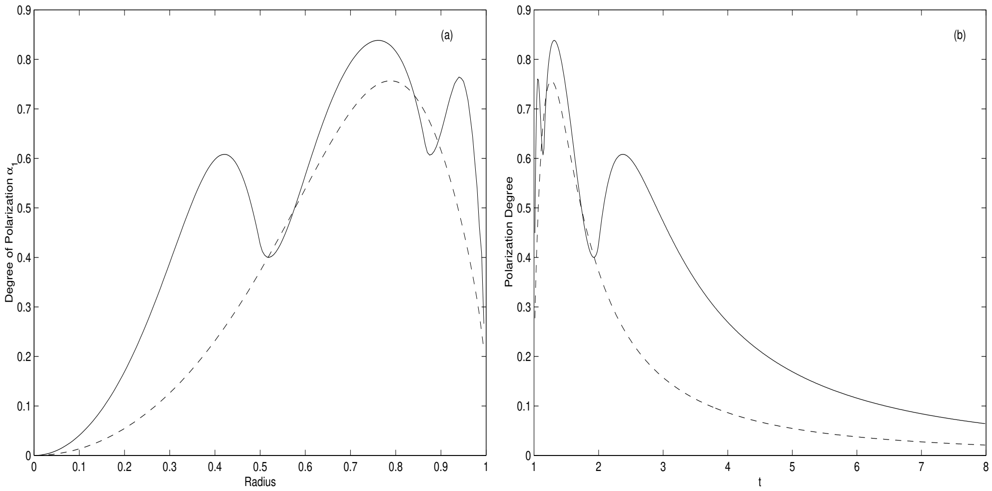

Figure 5. (a) Spatial distribution and (b) time traces of $\alpha_1^\mu(r,1)$ (solid line) and $\alpha_1^\rho(r,1)$ (dashed line).

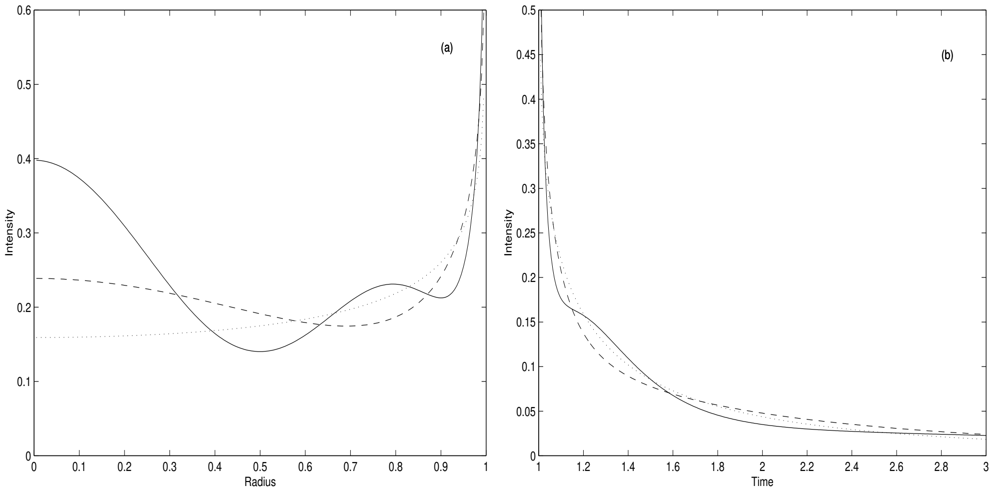

Figure 6. a) Spatial distribution at $t=1$ and (b) time evolution of the intensity at $r=1$ for the single scattering intensity $I(r,t)$ for the fluctuations in the Lamé parameters (solid line) Rayleigh (dashed line) and isotropic (dotted line) scattering.

5 NUMERICAL RESULTS IN SPHERICAL GEOMETRY

In this section we present Monte Carlo simulations for the energy density I and the degree of polarization $\alpha_1^{\mu,\rho}$ when multiple scattering is taken into account. We show a detailed analysis of the free space case. Some examples for the half-space and slab geometries are given in the next section.

In Fig. 7 we plot the spatial energy density distribution at different times. As in the previous section, the solution for the medium with fluctuating Lamé parameter μ (first case) is represented with solid lines, and the solution for the medium with fluctuating density ρ (second case) with dashed lines. The dotted lines correspond to the scalar isotropic

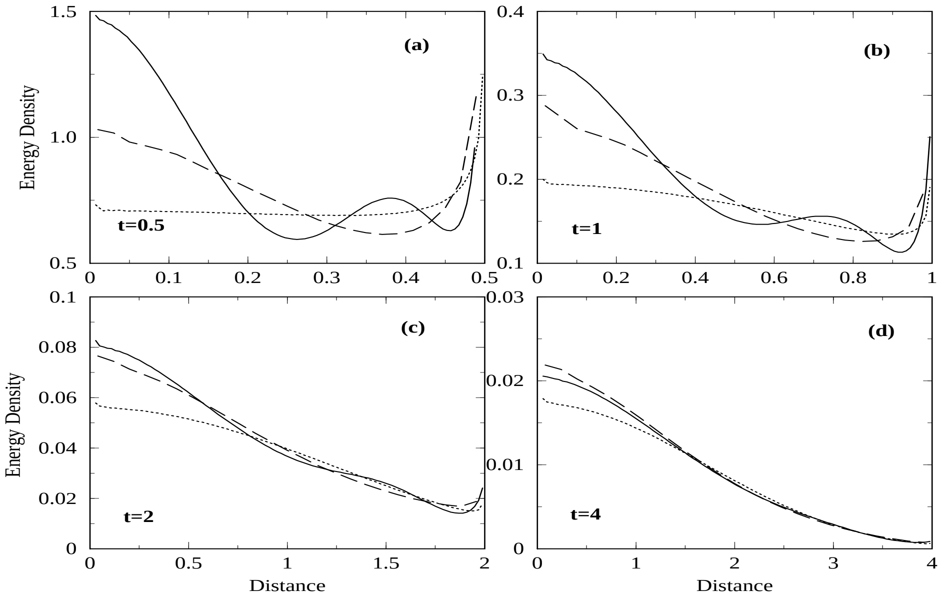

Figure 7. Spatial energy density distribution for a medium with $R_{\rho\rho} = 0$ (solid lines) and a medium with $R_{\mu\mu} = 0$ (dashed lines) at times $t = 0.5, 1, 2,$ and 4. Comparison with isotropic scattering (dotted lines).

scattering model, which is shown for comparison. The difference between the three cases is apparent for short lapse times [Fig. 7 (a)-(b)] and diminishes for larger times [Fig. 7(c)-(d)]. The reason is that single scattering is dominant for short times and the spatial energy density distribution strongly depends on the underlying scattering law as we have shown in the previous section. When time increases, multiple scattering destroys this effect, and all curves tend to the same diffusion solution.

More interesting for inversion problems [e.g., Wu, 1985; Fehler et al., 1992; Mayeda et al., 1992; Hosiba, 1995] are the time traces shown in Fig. 8. Again, we see that for small source-receiver distances, the early codas are not equal since high order multiple scattering is absent. However the late codas look alike. For large hypocentral distances the whole time traces are similar.

Hosiba, 1995, compares the early coda with the later one to estimate the amount of non-isotropy in scattering in western Japan. He found that the coda energy just after the S-wave arrival was more important than predicted by the isotropic scattering theory, so non-isotropy was introduced to explain this effect. Fig. 8(a)-(b) show that the total energy received during the early coda (i.e., $t < t_s$, where t_s is the S-wave travel time) depends on the scattering phase function. However, the observation of a large ratio between energies in the early and later coda cannot totally be explained by our model since we have assumed constant power spectra densities $\hat{R}_{\mu\mu}$ and $\hat{R}_{\rho\rho}$. Accounting for non-isotropic scattering is probably also necessary.

Fig. 9 and Fig. 10 describe the spatial distribution and time dependence of the degree of polarization, respectively. The solid lines represent case 1, and the dashed lines case 2. In Fig. 9(a), we recognize the already known spatial distribution profiles analyzed in section 4 for single scattering. The degree of polarization for fluctuating μ shows three peaks, the second of them coinciding in position and magnitude with the unique one for fluctuating ρ. Nevertheless, we observe in Fig. 9(b)-(d) that the closest peak to the source diminishes very quickly compared with the other two, and that the second peak is next

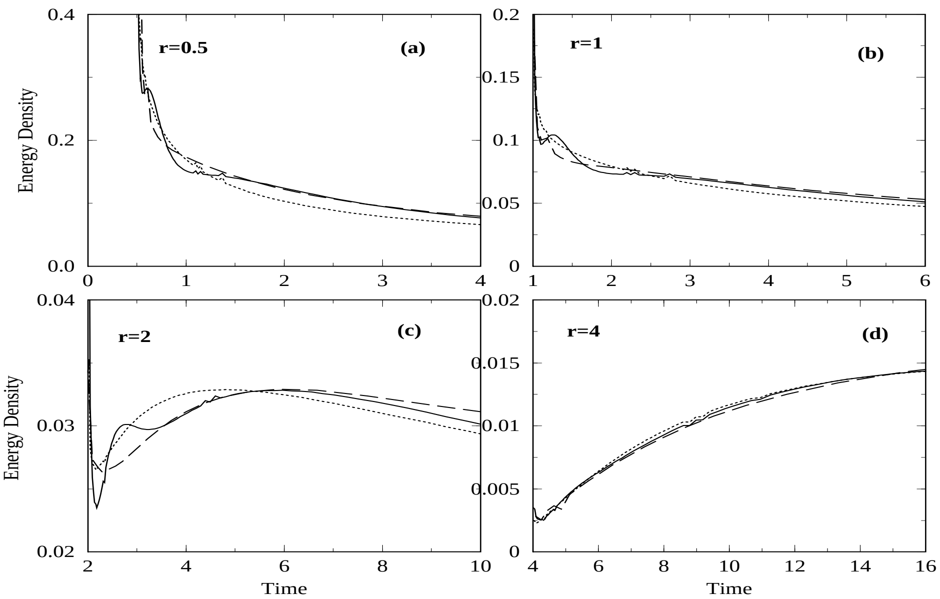

Figure 8. Time traces for a medium with $\hat{R}_{\rho\rho} = 0$ (solid lines) and a medium with $\hat{R}_{\mu\mu} = 0$ (dashed lines) at different distances from the source ($r = 0.5, 1, 2,$ and 4). Comparison with isotropic scattering (dotted lines).

to vanish. This effect is due to multiple scattering, which is responsible for depolarization. The closer we are from the source, the bigger the mean number of scattering events. On the other hand, we see that the polarization due to the interaction between the S-waves and the ρ inhomogeneity [dashed lines] remains longer in the medium. This last fact can be easily observed in Fig. 10, where we have plotted time traces for the rate of polarization. What is remarkable here, compared with Fig. 5(b) of section 4, is the fast decay of the polarization for the first case. This is explained in Fig. 11, where we have represented the spatial distribution of the degree of polarization of particles having 1, 2, 4, and 8 scattering events for both cases. This figure clearly shows that the depolarization due to the fluctuations of μ takes place much faster than the depolarization due to the fluctuations of ρ –only the waves closer to the first arrival remain more than 10% polarized after 8 scatterings–. Let us point out that the disagreement between the curve in Fig. 11(a) for one shock and the analytical curve calculated in the single scattering approximation [Fig. 5(a)] is due to the discretization of the angular direction; i.e., we have replaced the integral in equation (23) by a sum over 12 discrete directions. We checked that the agreement between both figures is better when we increase the number of discrete directions.

Fig. 8 and Fig. 10 show that the polarization is more sensitive than the energy density to the scattering phase function arising from different forms of fluctuations.

6 FREE SURFACE EFFECTS ON POLARIZATION

In this section, we analyze the effect on the degree of polarization of a perfectly reflecting horizontal interface. The main question is by how much the degree of polarization is modified by the interaction between incident and reflected waves. We have addressed the main differences between the two scattering phase functions coming from fluctuations of the Lamé parameter μ and the density ρ. We consider here only fluctuations of the density.

Fig. 12 depicts the degree of polarization for time $t = 2$. The non-polarized isotropic

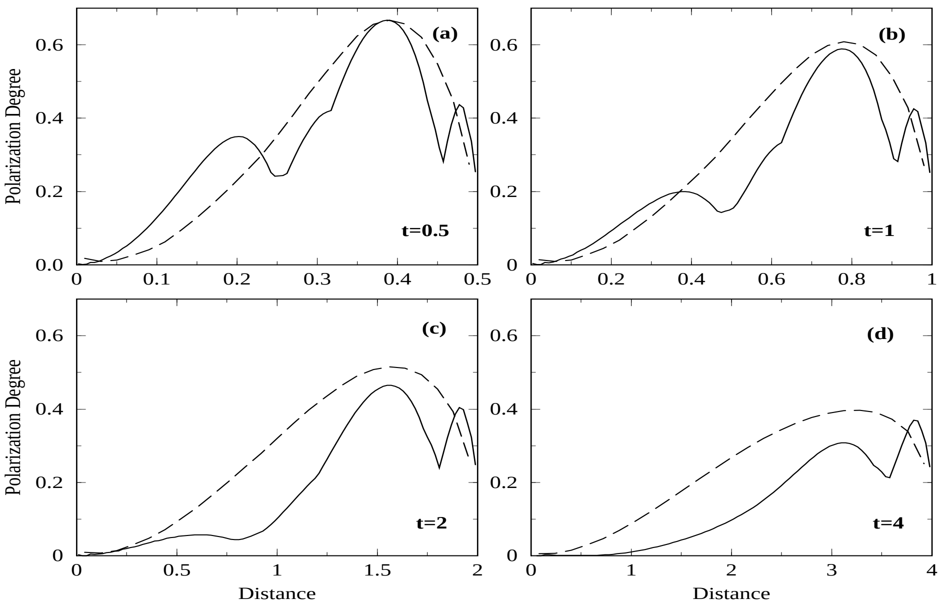

Figure 9. Spatial distribution of the rate of polarization for a medium with $\hat{R}_{\rho\rho} = 0$ (solid lines) and a medium with $\hat{R}_{\mu\mu} = 0$ (dashed lines) at times $t = 0.5, 1, 2$, and 4.

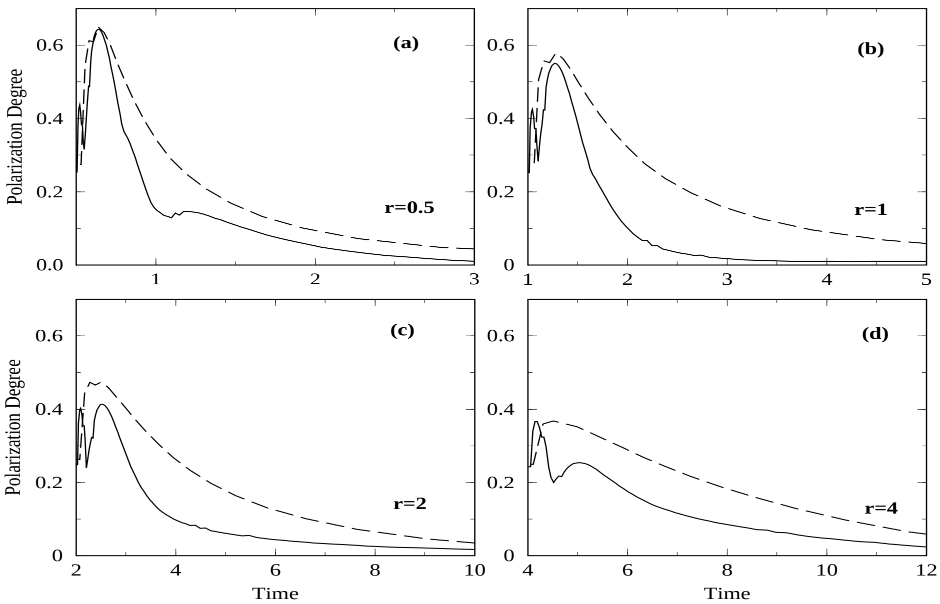

Figure 10. Time variations of the rate of polarization for a medium with $\hat{R}_{\rho\rho} = 0$ (solid lines) and a medium with $\hat{R}_{\mu\mu} = 0$ (dashed lines) at different distances from the source ($r = 0.5, 1, 2$, and 4).

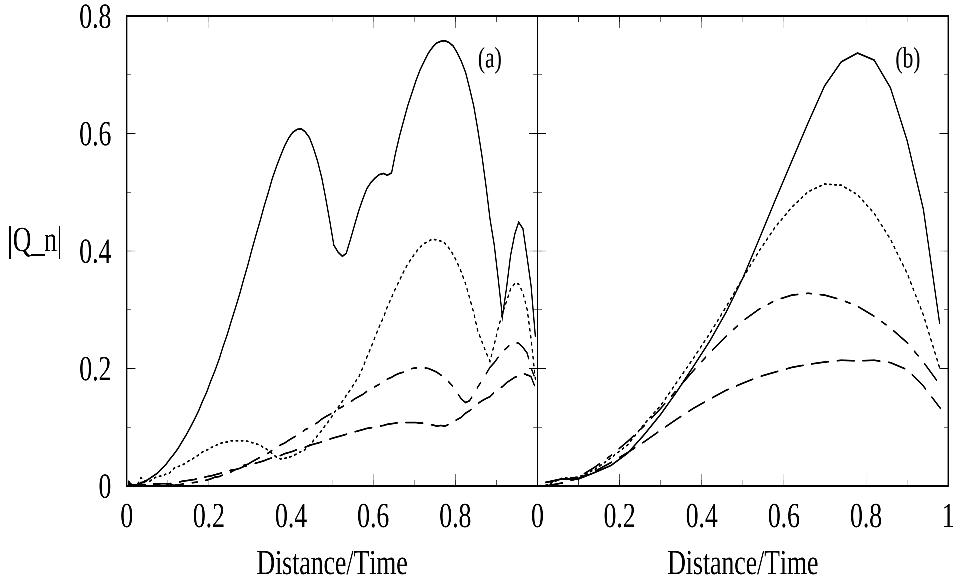

Figure 11. Spatial distribution of the degree of polarization of particles having 1 (solid line), 2 (dotted line), 4 (dash-dotted line) and 8 (dashed line) scattering events for (a) $\hat{R}_{\rho\rho} = 0$ and (b) $\hat{R}_{\mu\mu} = 0$.

point source is located at a distance $z = 1$ from the interface. Clearly, we can split the domain (r, z) into two areas. The lower part is actually identical to the spherical symmetry case, and corresponds to waves that did not see the interface. The maximum of the degree of polarization, about 0.5, agrees perfectly with the one shown in Fig. 9(c). The upper part corresponds to the area where some energy has been reflected from the free surface. We observe that the degree of polarization is lower than in spherical geometry. This is because the polarization of the reflected part adds destructively to that of the part which did not see the interface.

More interesting is the value of the degree of polarization at the surface, where it can be measured in practice. In Fig. 13, we see that in spite of the relative diminution of the polarization caused by the interface, we still observe a significant amount of polarized energy, at least for early times. As in the spherical geometry, the degree of polarization starts from zero, quickly grows until it reaches a maximum, and then slowly decreases back to zero for large times.

We have represented in Fig. 14 the degree of polarization at the free surface in slab geometry. The unpolarized source is 0.75 mean free paths away from the upper surface and 0.25 away from the lower interface, which is also assumed to be perfectly reflecting to simplify. As in Fig. 13, a first peak appears approximately 0.25 mean-free-times after the first arrival reaches the zero offset location. However, a second peak appears due to the energy which has been reflected from the lower boundary. Observe the presence of a minimum between these two maxima, where the degree of polarization is close to zero. This is explained by the unpolarized waves, which travel from the source to the lower boundary, are reflected and then received at the free surface.

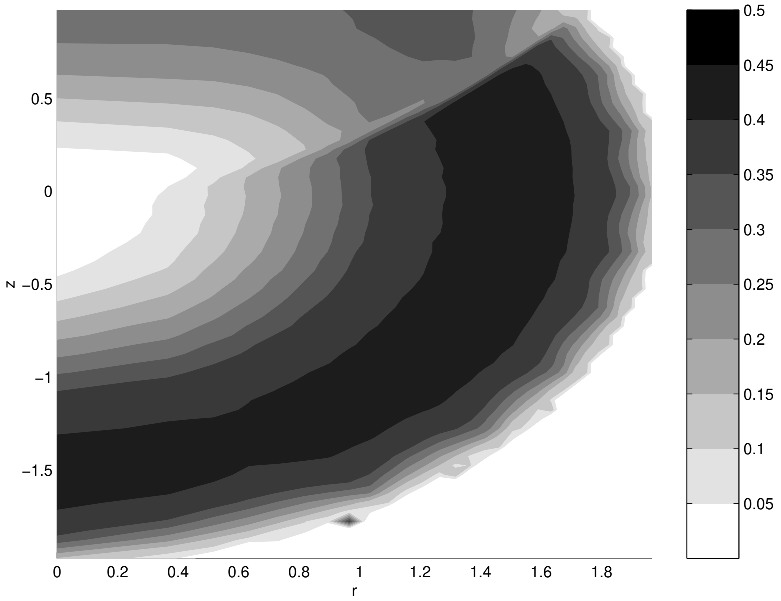

Figure 12. Degree of polarization in the half space geometry for a medium with fluctuations in the density. The non polarized isotropic point source is at $z = 0$ and the free surface is at $z = 1$.

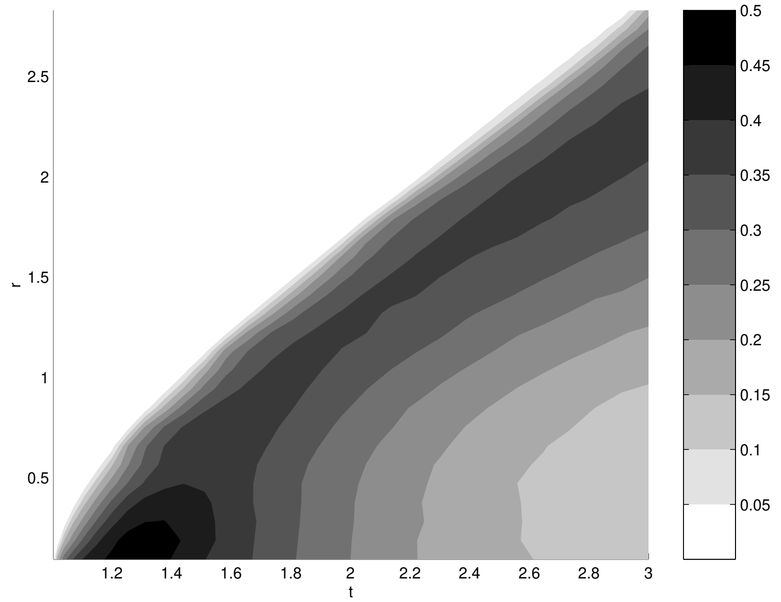

Figure 13. Degree of polarization at the surface for density fluctuations. The non polarized isotropic point source is at a distance $z = 1$ from the interface.

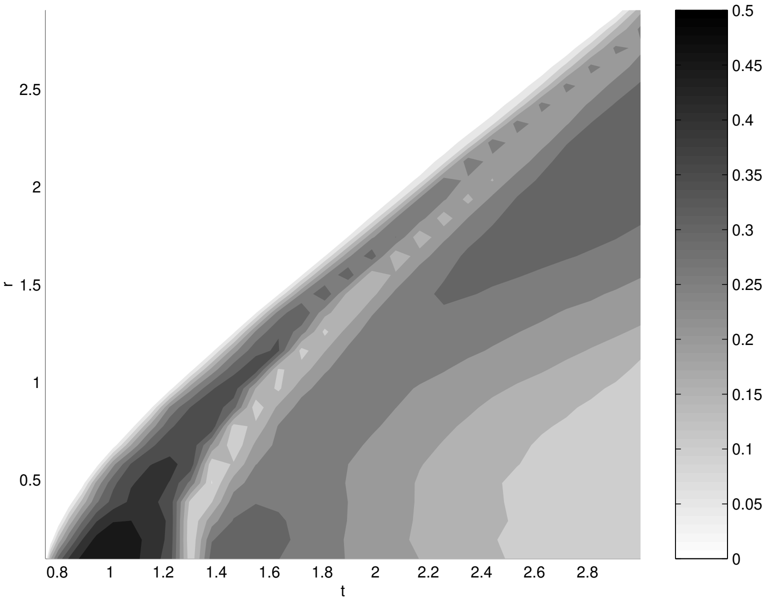

Figure 14. Degree of polarization pattern at the surface for the slab problem for a medium with fluctuations in the density. The non polarized isotropic point source is at a distance 0.75 from the surface and 0.25 from the lower boundary.

7 CONCLUSION

We have studied in this paper the polarization and depolarization effects of S-waves for media with fluctuating Lamé parameters or fluctuating mass density. The early coda for near-receivers is found to be very different for both cases and for the case of scalar isotropic scattering, whereas later codas and codas for far-receivers are similar. An analytical solution in the single scattering approximation has been presented for both cases. We found that the polarization effects are very important, and that the rate of polarization can be as large as 80% even for unpolarized sources. Besides, these effects are quantitative and qualitatively distinguishable for the two kinds of scattering phase functions considered. We have shown that both phenomena, polarization and depolarization of S-waves, take place faster in a medium with fluctuating Lamé parameters than in a medium with fluctuating density. We have also provided a Monte Carlo method for S-waves which is easy to implement and capable of solving general 3-D geometries. It now remains to investigate whether accurate estimates of the fluctuating properties of the Earth's lithosphere can be inferred from real seismic data.

For half-space and slab problems, we have shown that the presence of an interface lowers the degree of polarization. However, this degree remains clearly observable.

ACKNOWLEDGMENT

We would like to thank Joseph B. Keller, George Papanicolaou and Leonid Ryzhik for helpful discussions. This work has been supported by AFOSR grant 49620-98-1-0211 and by NSF grant 9709320.

APPENDIX A: PROBABILITY SCATTERING DENSITY

We give here an explicit expression for (16) and (17) for Rayleigh scattering. Let $S = T$ in these expressions. The components of the T matrix (6) are given by

$$\begin{aligned} T_{11} &= \cos\theta_k \cos\theta_{k'} \cos(\phi_k - \phi_{k'}) + \sin\theta_k \sin\theta_{k'}, \\ T_{12} &= \cos\theta_k \sin(\phi_k - \phi_{k'}), \\ T_{21} &= \cos\theta_{k'} \sin(\phi_{k'} - \phi_k), \\ T_{22} &= \cos(\phi_k - \phi_{k'}). \end{aligned} \tag{A.1}$$

Upon expanding the trace of TWT^*, we have

$$\pi(k,\mathcal{P},k',\mathcal{P}') = \frac{3}{16}\Big[\frac{T_{11}^2+T_{21}^2}{2}(1+p_1) + \frac{T_{12}^2+T_{22}^2}{2}(1-p_1) + (T_{11}T_{12}-T_{21}T_{22})p_2\Big]. \tag{A.2}$$

Then we have from (17)

$$\begin{aligned} p_1' &= \frac{8}{3\pi(k,\mathcal{P},k',\mathcal{P}')}\Big[\frac{T_{11}^2-T_{21}^2}{2}(1+p_1) + \frac{T_{12}^2-T_{22}^2}{2}(1-p_1) + (T_{11}T_{12}-T_{21}T_{22})p_2\Big] \\ p_2' &= \frac{8}{3\pi(k,\mathcal{P},k',\mathcal{P}')}\Big[T_{11}T_{21}(1+p_1) + T_{12}T_{22}(1-p_1) + (T_{11}T_{22}+T_{12}T_{21})p_2\Big]. \end{aligned} \tag{A.3}$$

For $S = \Gamma$, expressions (A.2) and (A.3) are the same but substituting $\Gamma_{ij} = T_{ij}$ $[(i,j) = 1,2]$ given by (6).

APPENDIX B: SINGLE SCATTERING INTENSITY AND POLARIZATION

The intensity which arrives at a point $\mathbf{r}$ after scattering at $\mathbf{r_1}$ under the Rayleigh's law is (see Fig. 2):

$$\frac{1}{4\pi r_1^2}\frac{1}{4\pi r_2^2}\frac{3}{4}(1+cos^2\Theta)\ . \tag{B.4}$$

The factors $1/4\pi r_1^2$ and $1/4\pi r_2^2$ in (B.4) come from the geometrical spread of the intensity from the source to the scatter and from this to the receiver, respectively. To obtain the total intensity at time t we have to integrate over all the space under the condition that the total travel time of the light is equal to t. Then,

$$\begin{aligned} I(\mathbf{r},t) &= \frac{3}{(8\pi)^2}\int \frac{1}{r_1^2 r_2^2}(1+cos^2\Theta)\delta(t-r_2-r_1)d\mathbf{r_2} = \\ &\quad \frac{3}{(8\pi)^2}\int_0^\infty\int_0^\pi\int_0^{2\pi}\frac{\delta(t-r_2-r_1)}{r_1^2 r_2^2}(1+cos^2\Theta)r_2^2 dr_2 sin\varphi d\varphi d\phi\ . \end{aligned} \tag{B.5}$$

Let us remark that

$$\begin{aligned} \delta(t-r_2-r_1) &= 2r_1\delta((t-r_2)^2-(r_1)^2) \\ &= 2r_1\delta((t-r_2)^2 - 2r_2(t-rcos\varphi)) \\ &= \frac{r_1}{t-rcos\varphi}\delta(r_2 - \frac{t^2-r^2}{2(t-rcos\varphi)}). \end{aligned}$$

Therefore, we have

$$I(r,t)=\frac{3}{32\pi}H(t-r)\int_0^\pi \frac{1}{r_1(t-rcos\varphi)}(1+cos^2\Theta)sin\varphi d\varphi \quad . \tag{B.6}$$

The numerator in (24) is the same as in (B.6) except for the positive sign in front of $cos^2\Theta$ replaced by a negative sign.

To integrate (B.6) it is more convenient to change to prolate spheroidal coordinates (ν,ω,ϕ) as in Sato & Fehler, 1998. The change of variables is the following:

$$x=\frac{r}{2}\sqrt{(\nu^2-1)(1-\omega^2)}cos\phi \; y=\frac{r}{2}\sqrt{(\nu^2-1)(1-\omega^2)}sin\phi \; z=\frac{r}{2}(1+\nu\omega) \; . \tag{B.7}$$

where r is the distance between the source and the receiver, and $\omega\in[-1,1]$, $\nu\in[1,\infty)$ and $\phi\in[0,2\pi]$. The Jacobian of this transformation is $\frac{rr_1r_2}{2}d\nu d\omega d\phi$ and

$$cos\Theta=\frac{2-\nu^2-\omega^2}{\nu^2-\omega^2} \; . \tag{B.8}$$

With these relations we end up with the integration of a rational function which can be performed trivially. The result for the total energy density in the case of fluctuating ρ is

$$I(r,t)=\frac{3}{16\pi r^2}\{\frac{3\nu^4-2\nu^2+3}{2\nu^5}\ln\frac{\nu+1}{\nu-1}+\frac{\nu^2-3}{\nu^4}\} \; . \tag{B.9}$$

APPENDIX C: IMPLEMENTATION OF THE MONTE CARLO METHOD

In this section, we describe the implementation of the Monte Carlo method for solving the radiative transfer equation (11).

C1 Decomposition in the number of scattering

Let us denote by

$$P(T,\mathbf{z},d\mathbf{z};\mathbf{z}_0) \tag{C.10}$$

the probability that a particle starting at time 0 from $\mathbf{z}_0=(\mathbf{x}_0,\mathbf{k}_0,\mathbf{p}_1^0,\mathbf{p}_2^0)$ be at time T at $\mathbf{z}=(\mathbf{x},\mathbf{k},\mathbf{p}_1,\mathbf{p}_2)$ about $d\mathbf{z}=d\mathbf{x}\,d\mathbf{k}\,d\mathbf{p}_1\,d\mathbf{p}_2$. We can decompose $P(T,\mathbf{z},d\mathbf{z};\mathbf{z}_0)$ over the number of scattering events between 0 and T as

$$P(T,\mathbf{z},d\mathbf{z};\mathbf{z}_0)=\sum_{n=0}^{\infty}Pr(T,N_s=n)\times P(T,\mathbf{z},d\mathbf{z};\mathbf{z}_0|N_s=n) \tag{C.11}$$

where N_s is the number of scattering events, or jumps, of the process $(X(t),Y(t))$ between 0 and T. Here $|$ means conditional expectation and $Pr(T,N_s=n)$ is the probability of having exactly n scattering events between 0 and T. In other words, the total probability density is decomposed over the number of scattering events that the process suffers between 0 and T. The Poisson distribution of the law of scattering times (15) allows one to compute each term in the sum (C.11) separately by Monte Carlo method. We can check that

$$Pr(T,N_s=n)=e^{-T}\frac{T^n}{n!}. \tag{C.12}$$

Moreover, for each number of scattering n, the times of scattering are obtained by increasing ordering of n values sampled between 0 and T with uniform distribution.

The first advantage in computing each term of the sum successively is the reduction of the statistical fluctuations. Indeed we include some information on the exact proportion of single scattering, double scattering, etc... in the total intensity. Moreover, we have access to those quantities and can easily obtain in which areas single scattering or multiple scattering is dominant. The second advantage is architectural. Our code is written in Matlab, which is much faster when properly vectorized. We calculate in turn the contributions of particles having exactly n scattering events during a fixed time T. Here, we have $1 \leq n \leq K$, where K is chosen so that the particles having more than K interactions during an interval of time of size T are negligible, i.e.

$$\sum_{n=K+1}^{\infty} e^{-T} \frac{T^n}{n!}$$

is small. Once n is fixed, the number of required operations to compute the trajectories of M particles is independent of the particle, therefore easily vectorized. The total number of particles $N = N_{loops} \times M$ is computed by N_{loops} successive calculations of packets of M particles.

For a fixed n, the operations required to simulate each trajectory are as follows. We first compute the times at which the process scatters. For each scattering we determine a new velocity k and new polarization parameters q and u of the outgoing particle according to Rayleigh scattering (16) and (17). As seen in (16), the probability distribution of the outgoing velocity depends on the incoming velocity, on the incoming polarization parameters, and on the outgoing velocity. It is however independent of the outgoing polarization parameters. The outgoing polarization parameters are determined by (17) once the outgoing velocity is known. Between scattering events, particles travel along straight characteristic with velocity $v = 1$.

C2 Spatial and Angular Discretization

Due to the large number of computations involved to simulate each trajectory, we have discretized the velocity and polarization spaces. We precompute the probability distribution of the outgoing parameters for these discrete values of the velocity and polarization. We then replace the exact Rayleigh probability distribution for the outgoing velocity by a piecewise constant probability distribution. Each interaction of a particle with the underlying medium is sampled accordingly.

At final time, the particles must be boxed to perform the averaging over the polarization parameters. We discretize the spatial domain with n_x boxes B_i, $1 \leq i \leq n_x$, and the angular domain with n_k directions k_l, $1 \leq l \leq n_k$. Each particle n for $1 \leq n \leq N$, is represented at final time T by $(\mathbf{x}(n), \mathbf{k}(n), q(n), u(n))$, which are its position, velocity, and polarization parameters, respectively. Then for each i and l, we compute the quantities

$$\begin{array}{rcl} I(i,l;T) & = & \sum_{n=1}^{N} \delta_{in}^{\mathbf{x}} \delta_{ln}^{\mathbf{k}} \\ Q(i,l;T) & = & \sum_{n=1}^{N} q(n) \delta_{in}^{\mathbf{x}} \delta_{ln}^{\mathbf{k}} \\ U(i,l;T) & = & \sum_{n=1}^{N} u(n) \delta_{in}^{\mathbf{x}} \delta_{ln}^{\mathbf{k}} \ , \end{array} \tag{C.13}$$

where

$$\delta_{in}^{\mathbf{x}} = \begin{cases} 1 \text{ if } \mathbf{x}(n) \in B_i \\ 0 \text{ otherwise} \end{cases} \qquad \delta_{ln}^{\mathbf{k}} = \begin{cases} 1 \text{ if } \mathbf{k}(n) \text{ is closer to } k_l \text{ than any other } k_j \\ 0 \text{ otherwise} \end{cases} \tag{C.14}$$

The quantities of interest are the intensity and the degree of polarization defined for each box by

$$I(i;T) \quad = \quad \frac{1}{N} \sum_{l=1}^{n_k} I(i,l;T) \tag{C.15}$$

$$\alpha_1(i;T) \quad = \quad \frac{\sum_{l=1}^{n_k} \sqrt{Q(i,l;T)^2 + U(i,l;T)^2}}{\sum_{l=1}^{n_k} I(i,l;T)}. \tag{C.16}$$

REFERENCES

Aki, K., 1969. Analysis of seismic coda of local earthquakes as scattered waves, *J. Geophys. Res.*, **74**, 615-631.

Aki, K. & Chouet, B., 1975, Origin of the coda waves: source, attenuation and scattering effects, *J. Geophys. Res.*, **80**, 3322-3342.

Aki, K., 1992. Scattering conversions P to S versus S to P, *Bull. seism. Soc. Am.,* **82**, 1969-1972.

Bal, G. & Moscoso, M., 1999. Theoretical and Numerical Analysis of Polarization for Time Dependent Radiative Transfer Equations, submitted to JQSRT.

Bal, G., Papanicolaou, G. & Ryzhik, L., 1999. Diffusion Approximation of Radiative Transfer Problems with Interfaces, to appear in SIAM Appl. Math.

Chandrasekhar, S., 1960. Radiative Transfer, Oxford University Press, Cambridge.

Fehler, M., Hosiba, M., Sato, H. & Obara, K., 1992. Separation of scattering and intrinsic attenuation for the Kanto-Tokai Region, Japan, using measurements of S-wave energy versus hypocentral distance, *Geophys. J Int.,* **108**, 787-800.

Frankel, A. & Wennerberg, L., 1987. Energy-flux model of seismic coda; Separation of scattering and intrinsic attenuation, *Bull. seism. Soc. Am.,* **77**, 1223-1251.

Gusev, A.A. & Abubakirov, I.R, 1987. Monte-Carlo simulations of record envelop of a near earthquake, *Phys. Earth Planet. Inter.,* **49**, 30-36.

Herraiz, M. & Espinosa, A.F., 1987. Coda Waves: A Review, *Pure Appl. Geophys.,* **125**, 499-577.

Hosiba, M. 1991. Simulation of multiple-scattered coda wave excitation based on the energy conservation law. *Phys. Earth Planet. Inter.,* **67**, 123-136.

Hosiba, M. 1995. Estimation of non-isotropic scattering in western Japan using coda wave envelopes: Application of a multiple non-isotropic scattering model, *J. geophys. Res.,* **100**, 645-657.

Ishimaru, A., 1978. Wave Propagation and Scattering in Random Media, Academic Press, New York.

Kalos,M. H. & Whitlock,P. A., 1986. Monte Carlo Methods, New York : J. Wiley Sons.

Margerin, L., Campillo, M. & van Tiggelen, B. A, 1998. Radiative Transfer and Diffusion of Waves in a Layered Medium: a New Insight into Coda Q, *Geophys. J Int.,* **134**, 596-612.

Mayeda, K., Koyanagi, S., Hosiba, M., Aki, K. & Zeng, Y., 1992. A comparative study of scattering, intrinsic, and coda Q^{-1} for Hawaii, Long Valley, and Central California between 1.5 and 15.0 Hz, *J. geophys. Res.,* **97**, 6643-6659.

Papanicolaou, G., Ryzhik, L. & Keller, J. B., 1996. Stability of the P to S energy ratio in the diffusive regime. *Bull. seism. Soc. Am.,* **86**, 1107-1115. Erratum, *Bull. seism. Soc. Am.,* **86**, 1997.

Ryzhik, L., Papanicolaou, G. & Keller, J. B., 1996. Transport equations for elastic and other waves in random media, *Wave Motion*, **24**, 327-370.

Sato, H., 1977. Energy propagation including scattering effect: single isotropic scattering approximation, *J. Phys. Earth*, **25**, 27-41.

Sato, H., 1984. Attenuation and Envelope formation of three-component seismograms of small local earthquakes in randomly inhomogeneous lithosphere. *J. geophys. Res.,* **89**, 1221-1241.

Sato, H., 1993. Energy transportation in one- and two-dimensional scattering media: Analytic solutions of the multiple isotropic scattering model, *Geophys. J Int.,* **112**, 141-146.

Sato, H., 1994. Formulation of the multiple non-isotropic scattering process in 2-D space on the basis of energy-transport theory, *Geophys. J Int.,* **117**, 727-732.

Sato, H. & Fehler, M. C., 1997. Seismic wave propagation and scattering in the heterogeneous earth, Springer-Verlag.

Shang, T. & Gao, L., 1988. Transportation theory of multiple scattering and its application to seismic coda waves of impulsive source, *Sci. Sin., Series B*, **31**, 1503-1514.

Spanier, J. & Gelbard, E. M., 1969. Monte Carlo principles and neutron transport problems, Reading, Mass., Addison-Wesley Pub. Co.

Tsujiura, M., 1978. Spectral analysis of coda waves from local earthquakes, *Bull. Earthquake Res. Inst. Univ. Tokyo*, **53**, 1-48.

Wu, R. S., 1985. Multiple scattering and energy transfer of seismic waves - Separation of scattering effect from intrinsic attenuation - I. Theoretical modeling, *Geophys. J. R. Astron. Soc.*, **82**, 57-80 .

Wu, R. S. & Aki, K., 1988. Multiple scattering and energy transfer of seismic waves- Separation of scattering effect from intrinsic attenuation - II. Application of the theory to Hindu-Kush region, *Pure Appl. Geophys.,* **128**, 49-80.

Zeng, Y., Su, F. & Aki, K., 1991. Scattering wave energy propagation in a random isotropic scattering medium 1. Theory, *J. Geophys. Res.*, **96**, 607-619.

Zeng, Y., 1993. Theory of scattered P- and S-wave energy in a random isotropic scattering medium. *Bull. seism. Soc. Am.,* **83**, 1264-1276.